2022 IEEE International Topical Meeting on Microwave Photonics (MWP) | 978-1-6654-2121-8/22/$31.00 ©2022 IEEE | DOI: 10.1109/MWP54208.2022.9997757

Design and Analysis of Low Bias, Low Phase Noise Photodetectors for Frequency Comb Applications Using Particle Swarm Optimization

Ishraq Md Anjum, Ergun Simsek, Seyed Ehsan Jamali Mahabadi, Thomas F. Carruthers, and Curtis R. Menyuk
Computer Science and Electrical Engineering
University of Maryland Baltimore County
Maryland, USA
ianjum1@umbc.edu

***Abstract*—We use particle swarm optimization to optimize the design of a low-bias (5 V) modified uni-traveling carrier photodetector for low-phase-noise frequency comb applications. We analyze the best design generated by the algorithm to determine the physics that leads to a phase noise reduction. We find that the phase noise can be reduced by increasing the electric field in the photon absorption region and by adjusting the doping levels and thicknesses of the layers in the intrinsic region to optimize the electric field.**

***Index Terms*—photodetectors, frequency combs, phase noise, evolutionary optimization algorithms**

I. Introduction

Low bias photodetectors are important because low bias reduces power consumption, simplifies the electronic design, and improves thermal performance [1]. Phase noise in photodetectors is a critical limiting factor in RF-photonics, time and frequency metrology, and photonic low-phase-noise microwave generation [2], [3]. We previously optimized a modified uni-traveling-carrier (MUTC) photodetector for low-phase-noise, high-bias (21 V) applications [4] using Nelder-Mead optimization; here we use particle swarm optimization (PSO) algorithm to find a better design for low-phase-noise, low-bias (5 V) applications, taking advantage of the PSO's ability to handle tens of parameters [5].

Achieving low phase noise with low bias is more difficult than when the bias is high [6]. Given the relationship between phase noise and the impulse response [7], it is possible to explain this. At low bias, the electric field in the intrinsic region is weaker. Hence, it takes the electrons a longer time to be swept across the photodetector when the bias is low than when it is high, which lengthens the tail of the impulse response and increases the phase noise [7].

There has been a large amount of work in the past five years that makes use of artificial intelligence and machine learning to gain insight into phenomena in nonlinear optics and photonics and to aid in system optimization [8], [9]. Evolutionary optimization algorithms have also become more widely used with newer algorithms like particle swarm optimization (PSO) increasingly displacing the older genetic algorithms [9]. The approach that works best is application-dependent, and some experimentation is required. In addition to optimizing the system design, the optimization algorithms can point out new, less obvious physics.

We apply the PSO algorithm— an evolutionary optimization algorithm to minimize the phase noise in a low power modified uni-traveling carrier (MUTC) photodetector that was designed by Li *et al.* [10] and was studied by Jamali *et al.* [7]. We use the one-dimensional (1-D) computational model based on the drift-diffusion equations that was developed by Hu *et al.* [11] and was improved upon by Simsek *et al.* [12] to calculate the impulse response of the photodetector.

In our optimization procedure, we modify both the device layer thicknesses and doping densities. Modifying these parameters modifies the electric field in the intrinsic region and suggests designs that sweep electrons through that region more quickly, Additionally, we found that increasing the electric field in the photon absorption region contributes to sweeping electrons out of the device more quickly and lowering the phase noise.

II. Phase Noise Calculation

It is possible to calculate phase noise in photodetectors using Monte Carlo simulations, [13] but that is computationally time consuming and is not suitable for optimization. Jamali *et al.* [7] calculated phase noise using the drift-diffusion equations by first calculating the impulse response and then noting that the electrons are Poisson-distributed in every time slot. In this work, we use the approach of Jamali *et al.* [7] to calculate the phase noise. In this approach, we first calculate the impulse response $h_e(t)$. Once we find $h_e(t)$, we use the equation [7]

$$\left\langle \Phi_n^2 \right\rangle = \frac{1}{N_{\text{tot}}} \frac{\int_0^{T_R} h_e(t) \sin^2\left[2\pi n(t-t_c)/T_R\right] \mathrm{d}t}{\left\{ \int_0^{T_R} h_e(t) \cos\left[2\pi n(t-t_c)/T_R\right] \mathrm{d}t \right\}^2} \tag{1}$$

to calculate the phase noise, where Φ_n^2 is the mean square phase fluctuation at comb-line number n, N_{tot} is the total number of electrons in the photocurrent, T_R is the repetition period, and t_c is the centroid time.

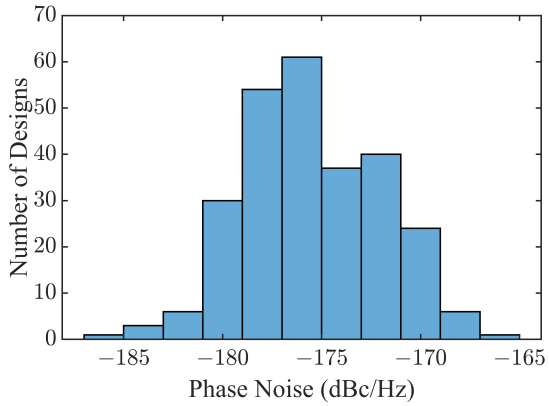

(a)

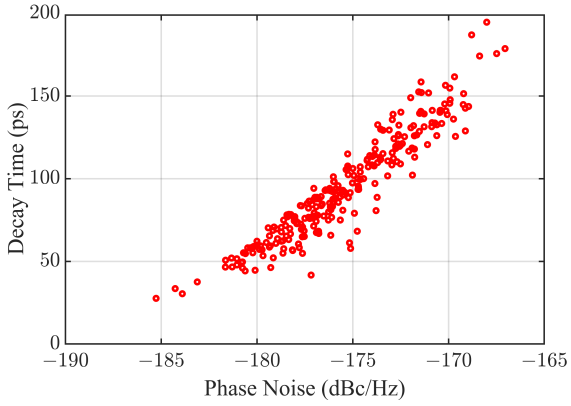

(b)

Fig. 1: (a) Phase noise histogram of the designs generated by the PSO algorithm. (b) Decay time vs. phase noise of the generated designs. Each red circle corresponds to a unique design generated by the PSO algorithm.

III. Optimization Process

Our starting point is the design of Li *et al.* [10] that was later studied by Jamali *et al.* [7]. The device has a diameter of 50 μm, the incoming light has a pulse-width 100 fs, a repetition frequency of 50 MHz, and an average current of 100 μA. In the Li *et al.* design [10], there are 17 layers, whose thicknesses and doping densities can be optimized. For the PSO algorithm, we use a swarm size of 400. Each of these swarm particles are candidate solutions, and they move around the solution space looking for the optimum combination of the parameters that would produce least phase noise. The absolute value of the difference between target phase noise and phase noise of the device under investigation is defined as the cost function to be minimized. We ran the optimization algorithm on a high performance computing cluster for 24 hours, and it generated around 300 designs out of which we chose the design with the least phase noise and adjusted the parameters to make the design suitable for fabrication and optimized it again, which reduced the phase noise even further.

In Fig. 1(a), we show the phase noise histogram and in Fig. 1(b), we show the scatter plot of decay time vs. phase noise of the designs generated by the PSO algorithm. We can see the positive correlation between phase noise and decay time [7] in Fig. 1(b). In Table I we list the doping densities and the thicknesses of the optimized MUTC photodetector. The changes are made in layers 6, 7, 8 and 12. Layer 12 in the original MUTC is merged with layer 13 in the optimized MUTC since the doping densities of the two layers are the same. We show the parameters that the PSO algorithm altered in boldface type. The device length of the original MUTC is 3230 nm whereas the device length of the new design is 2865 nm. The new device is about 10% thinner than the original device.

TABLE I: Material and doping types, doping concentrations, and layer thicknesses for the proposed design. Changes from the original design are indicated in boldface.

Layer No	Material and Doping Type	Doping Density (cm^{-3})	Thickness (nm)
1	InGaAs, p^+, Zn	2.0×10^{19}	50
2	InP, p , Zn	1.5×10^{18}	100
3	InGaAsP, Q1.1, p, Zn	2.0×10^{18}	15
4	InGaAsP, Q1.4, p, Zn	2.0×10^{18}	15
5	InGaAs, p, Zn	2.0×10^{18}	100
6	InGaAs, p, Zn	$\mathbf{1.0} \times 10^{18}$	**30**
7	InGaAs, p, Zn	$\mathbf{1.0} \times 10^{\mathbf{18}}$	**125**
8	InGaAs, p, Zn	$\mathbf{1.0} \times 10^{17}$	**230**
9	InGaAs, n, Si	1.0×10^{16}	150
10	InGaAsP, Q1.4, n, Si	1.0×10^{16}	15
11	InGaAsP, Q1.1, n, Si	1.0×10^{16}	15
12	InP, n, Si	1.0×10^{16}	**800**
13	InP, n^+, Si	1.0×10^{18}	100
14	InP, n^+, Si	1.0×10^{19}	900
15	InGaAs, n^+, Si	1.0×10^{19}	20
16	InP, n^+, Si	1.0×10^{19}	200
	InP (Substrate)		

In Figs. 2(a) and 2(b), we show the calculated impulse response of the photocurrent components, as the total normalized impulse responses of the original and optimized structure. In Figs. 3(a) and 3(b), we show the electric field distribution inside the original and the optimized MUTC. The calculated phase noise of the original and modified MUTC devices are -182.2 dBc/Hz and -186.6 dBc/Hz, respectively. The optimized MUTC has 4.4 dBc/Hz lower phase noise. The impulse response of the optmized MUTC has a shorter tail than the original, which contributes to the reduction of phase noise [7]. The original MUTC has a FWHM of 43.7 ps whereas the optimized MUTC has a FWHM of 27.3 ps. There is a reduction of 37.5% in the FWHM and a 22.3% reduction of decay time. The decay time is the time that it takes the impulse response to decay to 1% of its initial value. There is a 10% decrease in responsivity in the optimized device, which isn't large and is a tradeoff.

IV. Analysis of the Optimized Design

If we compare the electric field distribution in the intrinsic region of the original and optimized MUTC, we see that in the original MUTC, there is a low electric field region in

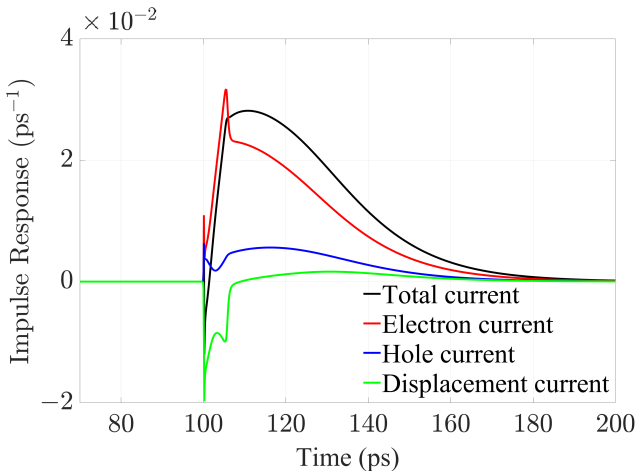

(a)

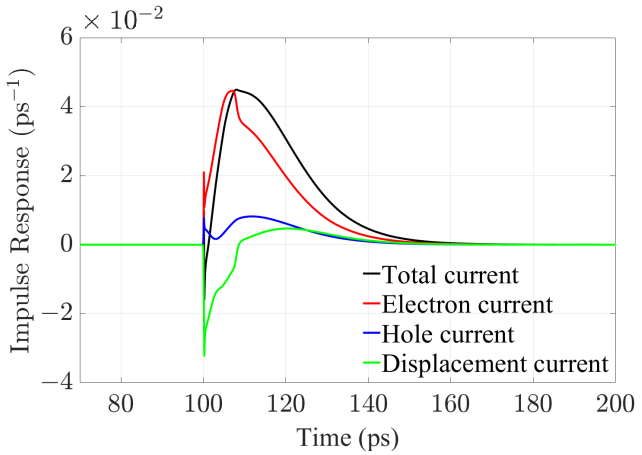

(b)

Fig. 2: Impulse response (a) of the original MUTC device and (b) of the new MUTC device

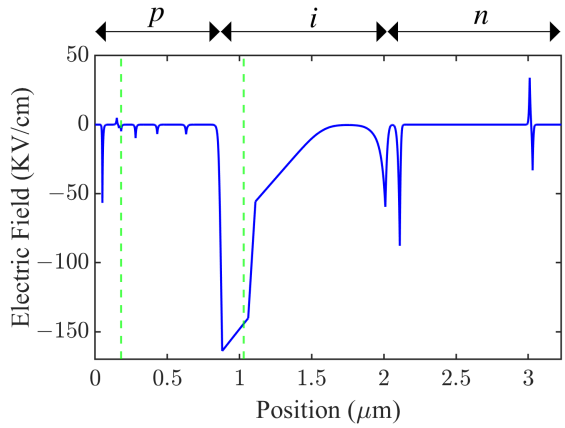

(a)

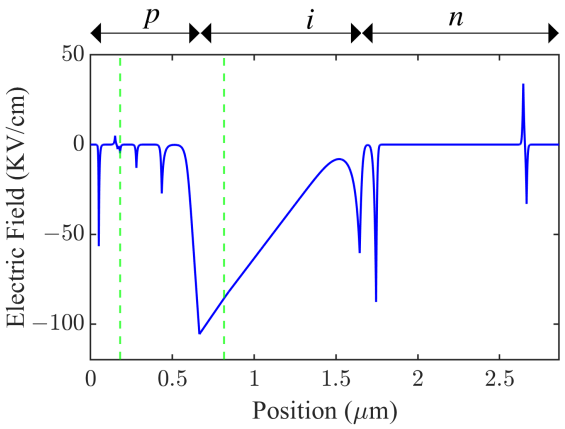

(b)

Fig. 3: Electric field at steady state inside the (a) original MUTC device and the (b) optimized MUTC device. Vertical dashed lines indicate the photon absorption region.

the 900-nm InP layer in the intrinsic region. In this region, the electron drift velocity cannot become large as the electric field is relatively small. As a result, the electrons slow down on their way towards the n-contact, which leads to a long tail in the impulse response. This region is a bottleneck. In the optimized MUTC, the low-electron-drift velocity region is not present since the electric field is larger in that region. The optimization algorithm obtained the larger electric field by decreasing the doping density of the 50-nm InP layer in the intrinsic region to 1.0×10^{16} and merging it with the 900-nm InP layer. Decreasing the doping density of the InP layer increases the electric field in that layer. We see in Fig. 4(a), which shows the electron drift current in the original design, the bottleneck in the electron drift current, while in Fig. 4(b), which shows our optimized design, the bottleneck is absent. We also see that the sharp decrease of the electric field that occurs in the 50-nm InP layer of the original MUTC design is absent in the optimized design, which leads to an overall larger electric field in the 800-nm InP layer in the optimized design.

There is a complex, nonlinear relationship between the electron drift velocity and the electric field. Our design optimization takes advantage of this complex relationship, and it is this complexity that makes computer optimization so effective. In InGaAs and InP, the electron drift velocity first rises as the electric field increases, but as electron drift velocity increases, the ratio of heavy (X- and L- valley) electrons to light (Γ-valley) electrons also increases, which then decreases the overall electron drift velocity [14]. As a result, the electron drift velocity reaches a maximum as the electric field increases and then decreases. The slope of the electron drift velocity changes, depending on the magnitude of the electric field. Photogenerated electrons and holes create an electric field that screens the pre-existing electric field in the device. Depending on the electric field in dark mode, the impact of the photo-generated electrons on the drift velocity changes because the derivative of the drift velocity with respect to the electric field changes. At points where the derivative is smaller, the electron transit time [6] varies less. Phase noise decreases when the variation of the electron transit time

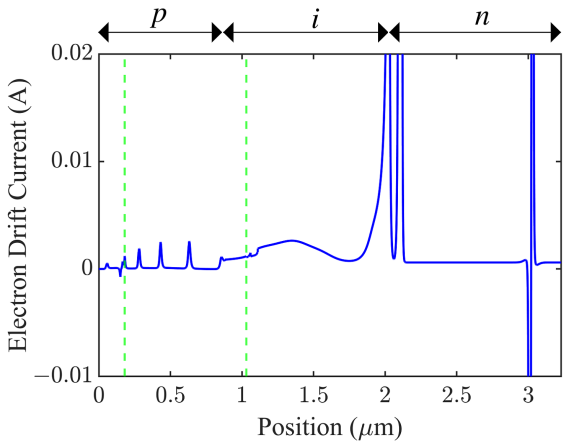

(a)

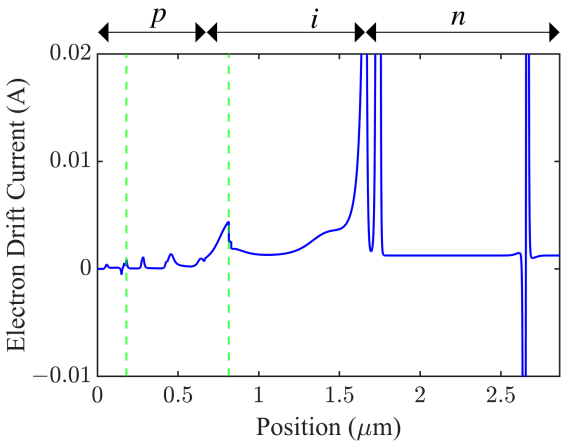

(b)

Fig. 4: Electron drift current inside (a) the original MUTC device and the (b) the optimized MUTC device. Vertical dashed lines indicate photon absorption region.

decreases. So, the overall higher electric field in the InP layer also contributes to the reduction of phase noise.

The PSO algorithm suggested changes in the doping densities and thicknesses of the three layers in the photon absorption region that led to larger electric fields at the layer boundaries. This increase in the electric field assists the electrons as they move from the absorption layers in the p-region into the intrinsic region. This increase also contributes to shortening the tail of the impulse response and decreasing phase noise.

The algorithm also suggested a decrease in the thickness of 900-nm InP layer to 800 nm. As a result, the time that it takes the electrons to cross the intrinsic region decreases, which shortens the tail of the impulse response. If the layer length decreases further, the electron RC transit time increases, which then again increases the total transit time and hence the tail of the impulse response. There is a tradeoff between photodetector length and transit time.

V. Conclusion

We have demonstrated that it is possible to optimize photodetectors using evolutionary optimization algorithm. The optimized MUTC device that the PSO algorithm found has 4.4-dBc/Hz lower phase noise than the original MUTC and is also thinner and faster. We used the optimized MUTC device that the algorithm found to infer the physics that led to lower phase noise.

Acknowledgment

A portion of our computational work was carried out at the UMBC High Performance Computing Facility (https://hpcf.umbc.edu).

References

[1] W. Liu, R. Cendejas, H. Cao, Q. Hang, Z. Ji and A. Nikolov, "Uncooled low-bias uni-traveling carrier photodetectors," CLEO: 2013, pp. 1–2, 2013.

[2] B. E. A. Saleh and M. C. Teich, *Fundamentals of Photonics* (Wiley, 1991).

[3] V. J. Urick, K. J. Williams, and J. D. McKinney, *Fundamentals of Microwave Photonics* (Wiley, 2015).

[4] E. Simsek, S. E. Jamali Mahabadi, I. M. Anjum and C. R. Menyuk, "Thinner and Faster Photodetectors Producing Lower Phase Noise," 2021 IEEE Photonics Conference (IPC), pp. 1–2, 2021.

[5] J. Kennedy and R. Eberhart, "Particle swarm optimization," *Proceedings of ICNN'95 - International Conference on Neural Networks,* vol. 4, pp. 1942–1948, 1995.

[6] J. Sun, B. Xu, W. Sun, S. Zhu and N. Zhu, "The Effect of Bias and Frequency on Amplitude to Phase Conversion of Photodiodes," *IEEE Photonics Journal,* vol. 12, no. 4, pp. 1–10, Art no. 5502010, Aug. 2020.

[7] S. E. J. Mahabadi, S. Wang, T. F. Carruthers, C. R. Menyuk, F. J. Quinlan, M. N. Hutchinson, J. D. McKinney, and K. J. Williams, "Calculation of the impulse response and phase noise of a high-current photodetector using the drift-diffusion equations," *Opt. Express,* vol. 27, no. 3, pp. 3717–3730, 2019.

[8] G. Genty, L. Salmela, J. M. Dudley, D. Brunner, A. Kokhanovskiy, S. Kobtsev, and S. K. Turitsyn, "Machine Learning and Applications in ultrafast photonics," *Nature Photonics,* vol. 15, no. 2, pp. 91–101, 2020.

[9] W. Ma, Z. Liu, Z. A. Kudyshev, A. Boltasseva, W. Cai, and Y. Liu, "Deep learning for the design of photonic structures," *Nature Photonics,* vol. 15, no. 2, pp. 77–90, 2020.

[10] Z. Li, H. Pan, H. Chen, A. Beling and J. C. Campbell, "High-Saturation-Current Modified Uni-Traveling-Carrier Photodiode With Cliff Layer," *IEEE J. Quantum Electron,* vol. 46, no. 5, pp. 626–632, 2010.

[11] Y. Hu, B. S. Marks, C. R. Menyuk, V. J. Urick, and K. J. Williams, "Modeling sources of nonlinearity in a simple PIN photodetector," *J. Lightw. Technol.,* vol. 32, pp. 3710–3720, 2014.

[12] E. Simsek, S. E. J. Mahabadi, I. M. Anjum, and C. R. Menyuk, "A Robust Drift-Diffusion Equations Solver Enabling Accurate Simulation of Photodetectors," PIERS 2021, Hangzhou, China, 21–25 November 2021.

[13] W. Sun, F. Quinlan, T. M. Fortier, J. D. Deschenes, Y. Fu, Scott A. Diddams, and J. C. Campbell, "Broadband noise limit in the photodetection of ultralow jitter optical pulses," *Phys. Rev. Lett.,* vol. 113, 203901, 2014.

[14] Y. Hu, C. R. Menyuk, X. Xie, M. N. Hutchinson, V. J. Urick, J. C. Campbell and K. J. Williams, "Computational Study of Amplitude-to-Phase Conversion in a Modified Unitraveling Carrier Photodetector," *IEEE Photonics Journal,* vol. 9, no. 2, pp. 1–11, Art no. 5501111, April 2017.